Pergamon

0022–5096(94)00071–9

SHEAR DOMINATED TRANSONIC INTERFACIAL CRACK GROWTH IN A BIMATERIAL—I. EXPERIMENTAL OBSERVATIONS

JOHN LAMBROS and ARES J. ROSAKIS

Graduate Aeronautical Laboratories, MS 105-50, California Institute of Technology, Pasadena, CA 91125, USA

ABSTRACT

In this work we describe a series of impact experiments performed on PMMA/4340 steel edge cracked bimaterial plates. Specimens were impacted at 20 m s^{-1} in a one point bend configuration using a high speed gas gun. Dynamic interfacial crack propagation was observed using the optical method of Coherent Gradient Sensing and high speed photography. Very high crack tip accelerations (10^8 m s^{-2}) and very high crack tip speeds (up to $1.5c_R^{PMMA}$) were measured and are reported. Quantitative measurements show that in experiments in which the crack tip speed entered the intersonic range for PMMA, the stress field surrounding the crack tip was shear dominated. The observation of high shear around the crack tip can also be explained using wave propagation arguments. It is found that the reason for attainment of intersonic (with respect to PMMA) crack tip speeds is directly related to the large amounts of energy necessary to initiate the crack tip under shear dominated conditions.

A comparison with the theoretical results of Part II in this study is also made. There seems to be an unfavorable region of stable crack propagation velocities in the intersonic regime. This region is $c_s^{PMMA} < v < \sqrt{2}c_s^{PMMA}$. In all experiments performed, the propagating crack accelerated quickly out of this region. In the few interferograms that do actually correspond to crack propagation in this unfavorable velocity range, crack face contact was observed. This observation is also in agreement with the findings of Part II of this investigation.

1. INTRODUCTION

In homogeneous materials transonic crack growth is defined as the regime in which a dynamically growing crack accelerates to propagation speeds that lie between the shear and dilatational wave speeds of the material (i.e. the intersonic region). In the area of homogeneous high speed fracture, there has been extensive theoretical work including the contributions of Burridge *et al.* (1979) and more recently of Broberg (1985, 1989), Bykovtsev and Kramarovskii (1989), Aleksandrov and Smetanin (1990) and Broberg (1993). However, as was shown by Broberg (1960) the speed of a remotely loaded traction free crack in a homogeneous material cannot exceed the Rayleigh wave speed c_R of that material. It was found there that an infinite amount of energy has to be transmitted to the crack tip to maintain extension at c_R if the stress intensity factor is non-zero [see also Freund (1990)]. This obviously makes it energetically impossible for a crack in a homogeneous solid to exceed the material's Rayleigh wave speed. For this reason it is difficult to obtain intersonic or supersonic

crack growth in homogeneous materials under laboratory conditions. Since it is energetically impossible for a remotely loaded crack to travel at speeds over c_R, the only way to observe such propagation is to directly supply energy to the crack by driving it externally. Examples of this include wedge opening of the crack faces or high energy laser pulse loading. Using laser pulse loading Winkler et al. (1970) and Curran et al. (1970) managed to drive cracks in KCl single crystals at supersonic speeds. These kinds of experiments are the only ones in which intersonic and supersonic crack growth have been recorded in a laboratory situation.

In recent years, there has been some interest in the phenomenon of dynamic interfacial fracture mechanics. Because of the intrinsic difficulties associated with this problem, only a few theoretical studies have been performed (Goldshtein, 1967; Brock and Achenbach, 1973; Atkinson, 1977; Willis 1971, 1973). Even so, it should be noted that there is a disagreement on the theoretically predicted value of the terminal velocity for dynamically propagating interfacial cracks. Atkinson (1977) claimed a terminal velocity equal to the lower of the Rayleigh wave speeds of the two constituents. In contrast Willis (1973) argued that the terminal velocity was a little greater than the lower of the two Rayleigh wave speeds. More recently the problem of dynamic interfacial crack growth has been studied by Yang et al. (1991) and Deng (1992). They provided a steady state asymptotic and higher order solution respectively for the stress field surrounding the tip of a dynamically propagating bimaterial crack. One very important conclusion of the study of Yang et al. (1991) is that as the crack tip velocity approaches the lower of the two Rayleigh wave speeds, $c_R^{(1)}$, a finite amount of energy has to be transmitted to the crack tip to maintain extension at $c_R^{(1)}$ with non-zero complex stress intensity factor (Fig. 1). The influence of transient effects in dynamic interfacial fracture was investigated by Liu et al. (1993). In their work they provide explicit expressions for the stress field around the tip of a transiently and dynamically propagating interfacial crack. In addition, experimental evidence corroborating the existence of very high crack tip accelerations and consequently very high transient effects was presented there. The validity of the theoretical analysis was also investigated by comparison with these experiments.

Up to this point, and to our knowledge, the only experimental studies on the subject of dynamic interfacial fracture mechanics are those of Tippur and Rosakis (1991), Liu et al. (1993) and Lambros and Rosakis (1994a,b). In Lambros and Rosakis (1994a) and Lambros and Rosakis (1994b) dynamic crack growth along a PMMA/ steel interface was seen to proceed at intersonic speeds (with respect to PMMA). This resolves the debate over whether the Rayleigh wave speed of the more compliant constituent of the interface represents an upper bound to possible crack propagation
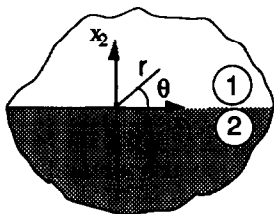

Fig. 1. Crack lying along a bimaterial interface.

velocities. It does not. In the current paper we will concentrate, for the first time, on the analysis of these transonic experiments. We will also provide a comparison with the theoretical results of the second paper (Part II) in this series.

2. EXPERIMENTAL TECHNIQUE AND OBSERVATIONS

2.1. *Coherent Gradient Sensing interferometer* (CGS)

The physical principle governing the optical method of CGS was first analysed by Tippur *et al.* (1991) and is described in detail by Rosakis (1993). Figure 2 is a schematic of the CGS arrangement in a transmission configuration. The bimaterial specimen shown is composed of a PMMA/steel combination. A coherent, mono-chromatic, collimated laser beam is incident on the deforming specimen. After trans-mission through the transparent (PMMA) side of the specimen, it acquires an optical path difference and loses collimation. The optical path difference acquired is due to stress induced changes in refractive index and due to a non-uniform contraction in the thickness direction around the vicinity of the crack tip (Poisson's ratio effect). The resulting, non-collimated, beam passes through two line diffraction gratings G_1 and G_2 of fine pitch p (typically 40 lines mm^{-1}). They are situated a distance Δ (typically 50 mm) apart and perform a shearing of the incident wave front. The gratings' output intensity is transmitted through a filtering lens L. A diffraction spot pattern is obtained on the filtering plane, which is located at the back focal plane of lens L. At this plane all but one diffraction orders are blocked. The one remaining diffraction spot (either of ± 1 orders), shown in Fig. 2 as the open circle on the
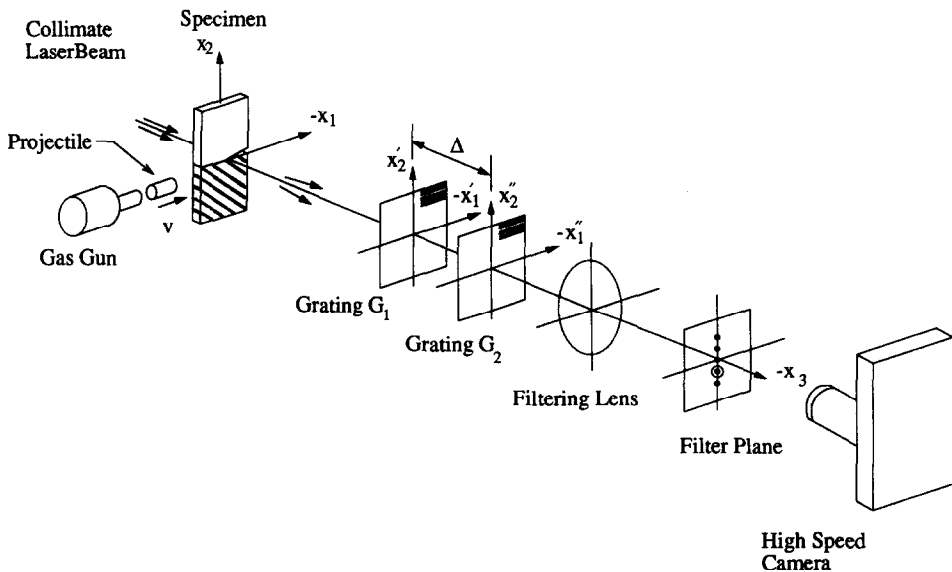

Fig. 2. Schematic of CGS set-up in transmission. PMMA/steel bimaterial specimen is illustrated.

filtering plane, is imaged to produce an interference pattern. For the case of a dynamic experiment the imaging device is a high speed camera focused on the specimen.

For the sake of simplicity and brevity we will not present the details of analysing the CGS optical method. These details can be found in several previous articles including Tippur et al. (1991) and Rosakis (1993). In addition a derivation of the CGS interferometric formulas using analyses based on Fourier optics can be found in Tippur (1992) and Lee et al. (1994). The condition for formation of constructive CGS interference fringes on the image plane is,

$$\frac{\partial(S(x_1, x_2))}{\partial x_1} = \frac{mp}{\Delta}, \quad m = 0, \pm 1, \pm 2, \ldots. \tag{1}$$

In the above equation $S(x_1, x_2)$ is the optical path change of the originally collimated laser beam, that has been introduced by the specimen deformation. It has also been assumed that the diffraction gratings G_1 and G_2 are close enough and/or fine enough to obtain an interferogram that represents the x_1-gradient of S (rather than an x_1 finite difference of S). If the grating lines are parallel to the x_1 direction then it can be shown that the condition for constructive interference becomes

$$\frac{\partial(S(x_1, x_2))}{\partial x_2} = \frac{np}{\Delta}, \quad n = 0, \pm 1, \pm 2, \ldots. \tag{2}$$

For solid mechanics applications, it is desirable to relate the quantity $S(x_1, x_2)$ to the stress state in the deforming specimen. Such a relation is discussed in detail in Rosakis (1993) and will not be presented here. For linearly elastic, isotropic bimaterial specimens of finite thickness, Lee and Rosakis (1993) have investigated the extent of the region of three dimensionality in the vicinity of the crack tip. They have also identified regions surrounding the tip where a plane stress approximation is valid. In such regions the optical path difference $S(x_1, x_2)$ can be expressed as,

$$S(x_1, x_2) \approx c_\sigma h \left[\hat{\sigma}_{11}(x_1, x_2) + \hat{\sigma}_{22}(x_1, x_2) \right], \tag{3}$$

where c_σ is a stress optical coefficient for the material, h is the specimen thickness and $\hat{\sigma}_{11}$ and $\hat{\sigma}_{22}$ are thickness averages of the in-plane stress components in the plate.

For points outside the near tip three dimensional region the CGS patterns assume a simple interpretation in terms of two dimensional stress field approximations. In particular, (1) and (2) in conjunction with (3) now indicate that the fringes obtained from regions surrounding the three dimensional zone can be related to the in-plane gradients of $\hat{\sigma}_{11} + \hat{\sigma}_{22}$ as follows:

$$c_\sigma h \frac{\partial(\hat{\sigma}_{11} + \hat{\sigma}_{22})}{\partial x_1} = \frac{mp}{\Delta}, \quad c_\sigma h \frac{\partial(\hat{\sigma}_{11} + \hat{\sigma}_{22})}{\partial x_2} = \frac{np}{\Delta}, \quad m, n = 0, \pm 1, \pm 2, \ldots, \tag{4}$$

where in the case of transmission c_σ is the stress optical coefficient of the transparent material (PMMA).

2.2. Bimaterial experiments

In order to intensify dynamic effects at the interface, it was decided to use bimaterial constituents that have a very large mechanical property mismatch. To be able to use a transmission CGS arrangement in our experimentation, one side of the bond,

the more compliant side, was chosen to be Plexiglas (Poly-Methylmethacrylate or PMMA). The other side of the bond was chosen as AISI 4340 steel which is considerably stiffer and tougher than Plexiglas. It also has wave speeds which are considerably larger than those in polymers. Throughout this study, the PMMA side of each specimen will be referred to as material-1 and the metal side as material-2. So with reference to Fig. 1, the more compliant material occupies the positive x_2-plane.

The mechanical properties of the constituents are shown in Table 1. It also shows the value of the plane stress quasi-static oscillatory index ε for the bimaterial combination of PMMA/steel ($\varepsilon^{P/S}$) and of Plexiglas bonded to a rigid substrate ($\varepsilon^{P/R}$). As can be seen, these values are extremely close. This would suggest that we can expect intense interfacial effects during the dynamic fracture event. It also justifies the comparison of the experimental results with the elastic–rigid analysis presented in Part II of this study.

The specimen preparation procedure follows the lines of Tippur and Rosakis (1991) and will not be described here. The crucial issue of bond strength has also been addressed by the performance of bond calibration tests by Tippur and Rosakis (1991). In those tests it was shown that the fracture toughness of two bonded PMMA halves was over 95% of that of homogeneous PMMA. Additional quasi-static crack growth tests in PMMA/steel three point bend edge cracked plates were performed in Lambros and Rosakis (1994b). In those experiments it was seen that the measured quasi-static initiation toughness was about 1.1 MPa m$^{1/2}$. This value is also over 95% of the toughness of homogeneous PMMA. This testifies that the toughness of the PMMA and steel bond is at least as much as that of homogeneous PMMA.

The impact experiments performed in this study were of the one point bend type. The specimens used had a width of 127 mm, a total length of 305 mm and nominal thickness of 9 mm. Either a sharp edge crack or blunt notch (750 μm wide) was introduced along the interface. The length of the precrack in all cases was 25 mm. The loading device used was a high speed gas gun. The gun launches a cylindrical steel projectile 75 mm long and 50 mm in diameter. In all cases an impact velocity of 20 m s^{-1} was used. Because the wave speeds of PMMA and steel are significantly different, the loading history experienced by the crack tip would differ depending on which side of the specimen were impacted. For consistency with earlier low impact

Table 1. *Mechanical properties of interface constituents*

Property	PMMA	AISI 4340 Steel
E (GPa)	3.24	208
v	0.35	0.3
c_l (m s^{-1})	2080	5970
$c_l^{pl-\sigma}$ (m s^{-1})	1760	5400
c_s (m s^{-1})	1000	3190
c_R (m s^{-1})	935	2950
ρ (kg m^{-3})	1190	7830
$\varepsilon^{P/S} = 0.1037$		$\varepsilon^{P/R} = 0.1073$

speed tests performed in a drop weight tower (Lambros and Rosakis, 1994a,b) and to avoid shattering the PMMA side of the specimen, it was chosen to always impact the steel side (see Fig. 3).

A short time after impact, about 30 μs, the precrack lying on the interface initiates and a dynamic crack propagates along the interface. The technique of CGS in transmission was used in conjunction with high speed photography to record dynamic crack tip fields in a region surrounding the propagating crack. The light source used was a Spectra-Physics argon-ion pulsed laser (model 166-09) operating at a wavelength of $\lambda = 514.5$ nm (green light). Since PMMA is transparent and steel opaque to this wavelength, only half the laser beam exits the specimen. We are therefore able to record deformation fields only in the PMMA half of the specimen. After emergence from the specimen, the beam is processed by two diffraction gratings (see Fig. 2) located at a distance $\Delta = 50$ mm apart. They are Ronchi line gratings on glass with a 40 line mm^{-1} ruling. This corresponds to a pitch $p = 0.0254$ mm. The angular sensitivity of the interferometer with these settings is 0.015° (fringe)$^{-1}$. The imaging medium used in the experiments was a rotating mirror type high speed camera (Cordin Co., model 330A). Filtering of the $+1$ or -1 diffraction orders was performed internally in the camera using appropriate optics. The camera was typically run at an interframe time of 1.2 μs (about 840,000 frames s^{-1}). Individual frames were obtained by operating the laser light source in a pulsed mode. The exposure time used in all experiments (i.e. the laser pulse duration) was 30 ns. However, because of light losses in the optical components, very sensitive 35 mm black and white film was used (Kodak TMAX-3200). Because the total number of frames obtainable by this camera is 80, at a framing rate of 1.2 μs the total image recording time is about 95 μs. This means that precise triggering of the laser is very important. A strain gauge placed on the specimen at the point of impact senses the impacting projectile, and its signal is used to initiate pulsing of the light source.
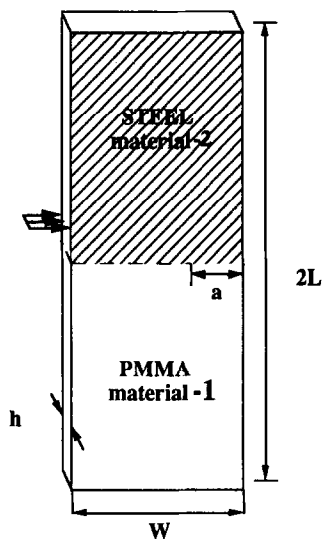

Fig. 3. One point bend impact geometry.

A typical selected sequence of interferograms from a one point bend experiment on a PMMA/steel specimen containing a sharp edge crack is shown in Fig. 4. Of course only the PMMA side of the specimen is shown. A sequence of interferograms from an experiment were a blunt starter notch was used, is seen in Fig. 5. The notch is visible in the lower left hand corner of the first frame shown. A residual stress field surrounding what used to be the notch tip can be seen in the lower left hand corner of the last frame in Fig. 5. One of the differences between these two kinds of experiments is that in cases where a blunt starter notch was used as an initiator, crack tip speeds were higher on average. Details of these experiments will be analysed in the next section and discussed in Section 3.

2.3. *Experimental observations*

Typical crack tip speed histories from two nominally identical one point bend gas gun tests are shown in Fig. 6(a) and (b). Both these are from specimens containing a sharp starter crack. The crack tip speed was determined by fitting a high order polynomial expression to the experimentally recorded crack length history. It can be seen that in both cases the crack tip speed rises very quickly (between 5 and 10 μs) to a value of around 1000 m s^{-1}. This is very close to the shear wave speed of PMMA (see Table 1). The most notable feature of the curves in Fig. 6 is the distinct plateau just after the crack speed has reached c_s^{PMMA}. The velocity then remains constant at this value (1000 m s^{-1}) for about 15 μs, after which time it seems to again rise sharply. The reason for the deceleration and plateau will become clear in the discussion section of this paper when the experimental results are related to the theoretical conclusions of Part II of this investigation. In any case the existence of a velocity plateau is a very repeatable feature of the experimental measurements as is illustrated by the very similar results of two different tests in Fig. 6. One other notable point is that in both the initial and subsequent acceleration regions the crack tip acceleration is estimated to be around 10^8 m s^{-2}. This suggests a highly transient fracture event. The high acceleration region following the velocity plateau is also a very repeatable feature of the experiments.

In all gas gun tests it was seen that the Rayleigh wave speed of PMMA, c_R^{PMMA}, had definitely been exceeded by the propagating crack tip. As was mentioned earlier, this resolves the debate as to whether c_R^{PMMA} is the limiting speed for dynamic crack propagation along the PMMA/steel interface. In addition we see from Fig. 6 that towards the end of our observation window the crack tip speed reaches values of about 1500 m s^{-1}. This is a significant fraction (85%) of the plane stress dilatational wave speed of PMMA. It shows that unassisted crack growth in the intersonic regime for PMMA is possible under the particular configuration and loading used in this experiment. Recall that the slowest wave speed in steel, its Rayleigh wave speed, is about 3000 m s^{-1}, i.e. considerably more than the crack tip propagation speed. With respect to the steel side of the bond, the crack tip speed is 0.5 c_s^{STEEL}. In the future it is planned to shift the observation window in our experiments in order to capture the later stages of crack propagation and thus possibly measure the terminal crack tip speed for this bimaterial system.

Additional evidence of crack propagation in the intersonic regime for PMMA can

be found by a visual investigation of the fringe patterns in Figs 4 and 5. In Fig. 5 for example, it is clear that the nature of the fringe pattern in the first and last frames is completely different. At first the fringes are smooth and continuous. They somewhat resemble the fringe patterns obtained in lower impact speed tests conducted by Lambros and Rosakis (1994b). Note that in those lower impact speed tests the crack propagation speed was subsonic throughout the test. In subsequent frames of Fig. 5 however, we see the fringes become squeezed and elongated in the x_2 direction (normal to the crack line). This is visual evidence that the stress field is drastically changing, and it is believed to be a velocity effect that is causing the fringe elongation (see the theoretically predicted fringe pattern in Fig. 5 of Part II of this study). At even later stages of crack growth, kinks appear in the previously smooth fringes. In the last frame of Fig. 5 (also shown enlarged in Fig. 7) we see a fringe pattern that is substantially different to those at lower crack tip speeds. The fringes in the center of the two lobed fringe pattern do not seem to focus to a single point along the interface. Instead they intercept the bond line over a finite area between the two main lobes, and even form closed, narrow loops, distinct from the overall fringe pattern. This effect is seen clearly in Fig. 7, in which the length of the area between the front and back lobes is identified as d. It is believed, based on the results of the theoretical analysis of Part II, that the fringe pattern seen in this particular frame is caused by contact of the crack faces along d, as the crack is propagating. This subject is still under investigation and will be explained more in the next section. However, what is absolutely clear to us at this point is the crack propagation speed has definitely exceeded both the Rayleigh and the shear wave speeds of PMMA and this coincides with drastic changes in the fringe pattern. It should also be noted that the interference patterns shown in Fig. 4, which correspond to crack growth velocities up to c_s^{PMMA}, do not seem to exhibit this effect. Instead fringes between the front and back lobes seem to focus at a single point, the crack tip.

3. RESULTS AND DISCUSSION

3.1. *Qualitative features of experiments*

The duration of a typical experiment of a gas gun loaded bimaterial plate was about 50–60 μs from impact until the crack ran out of our field of view. Crack initiation occurred about 30 μs after impact. These are relatively short times, during which waves propagating in PMMA travel a very small distance compared to waves propagating in steel. Therefore in the time frames involved in these experiments, the loading history at the initial crack tip is primarily due to waves traveling in steel. The effects visible on the PMMA side of the specimen are because of energy transferred across the interface from the steel side and from diffraction at the initial crack tip. In the 30 μs to initiation a wave generated at impact and traveling in the PMMA side covers a distance of only 60 mm. This is less than half the specimen height. Clearly therefore the initiation and early stages of the propagation process are driven by energy being transferred from the steel side across the interface. Because the Rayleigh wave speed of steel is larger than even the dilatational wave speed of Plexiglas, it is
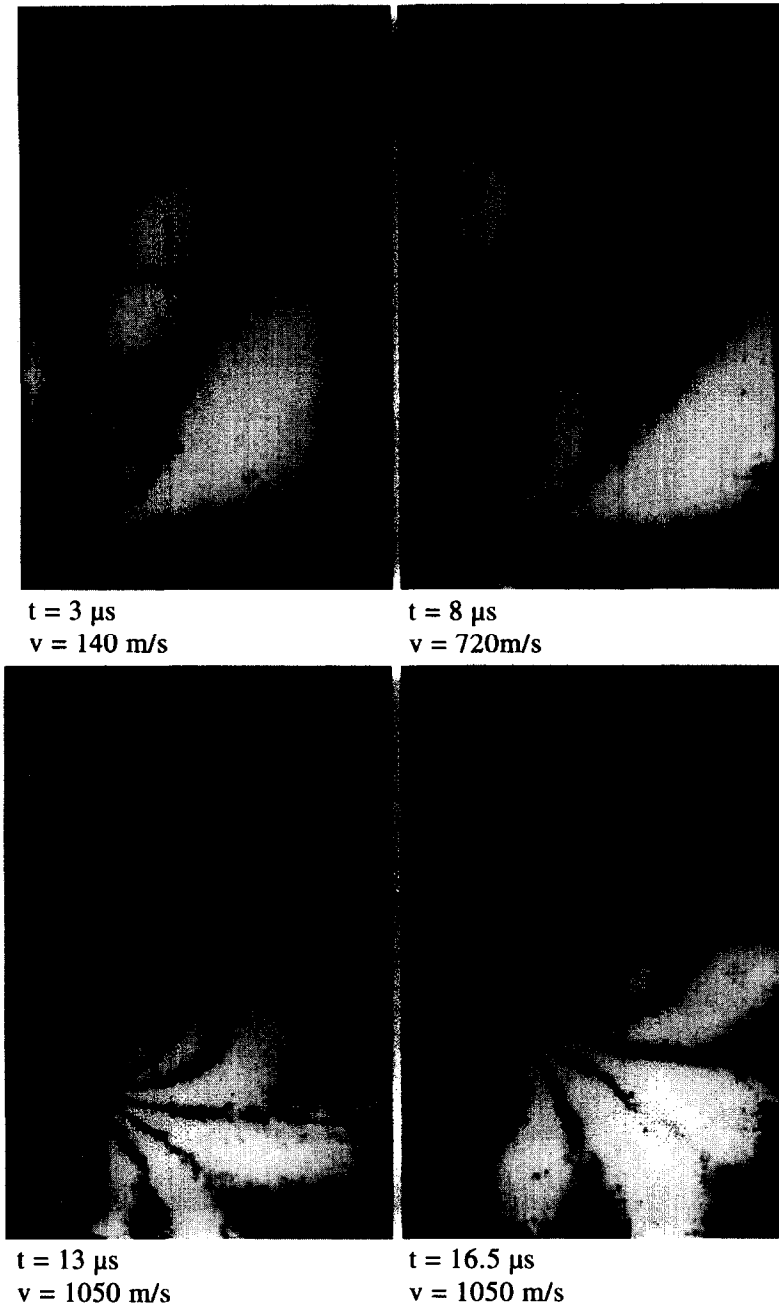
t = 3 µs
v = 140 m/s

t = 8 µs
v = 720m/s

t = 13 µs
v = 1050 m/s

t = 16.5 µs
v = 1050 m/s

Fig. 4. Selected sequence of CGS interferograms obtained from a one point bend air gun test on a PMMA/steel specimen (sharp starter crack used).
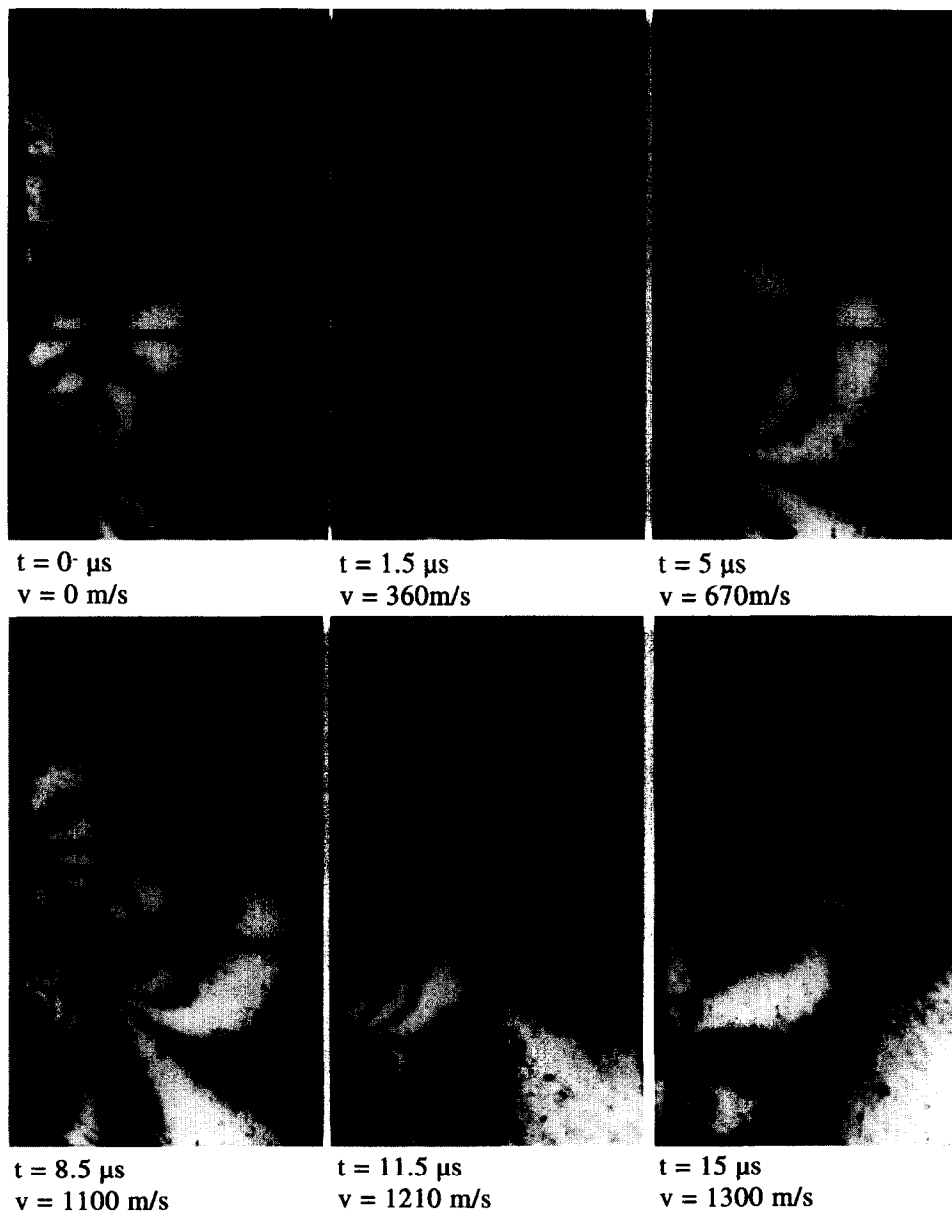
J. LAMBROS and A. J. ROSAKIS

t = 0⁻ μs
v = 0 m/s

t = 1.5 μs
v = 360m/s

t = 5 μs
v = 670m/s

t = 8.5 μs
v = 1100 m/s

t = 11.5 μs
v = 1210 m/s

t = 15 μs
v = 1300 m/s

Fig. 5. Selected sequence of CGS interferograms obtained from a one point bend air gun test on a PMMA/steel specimen (blunt starter notch used).

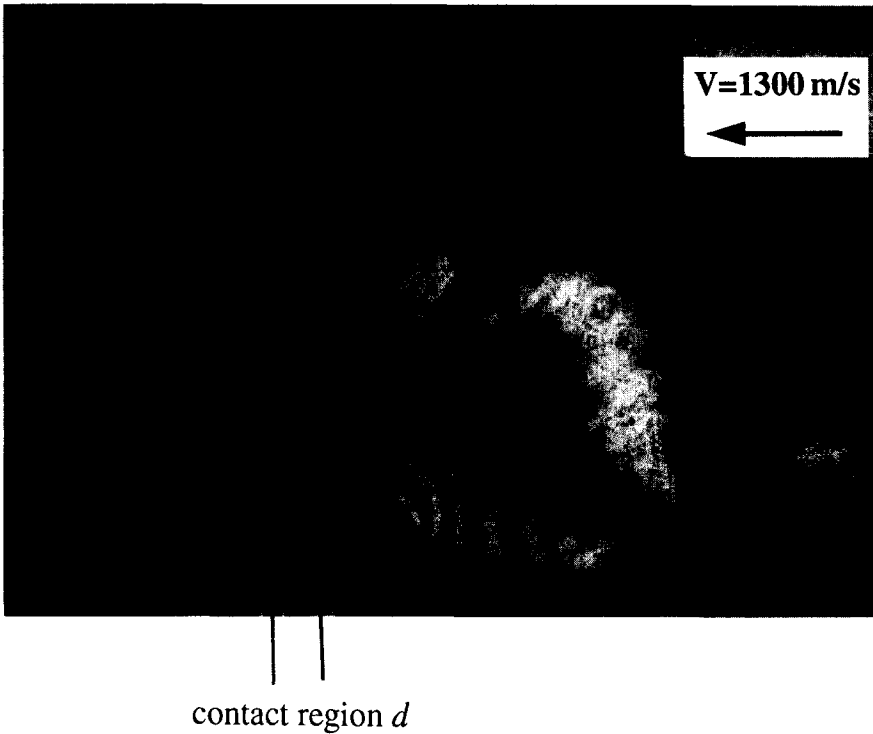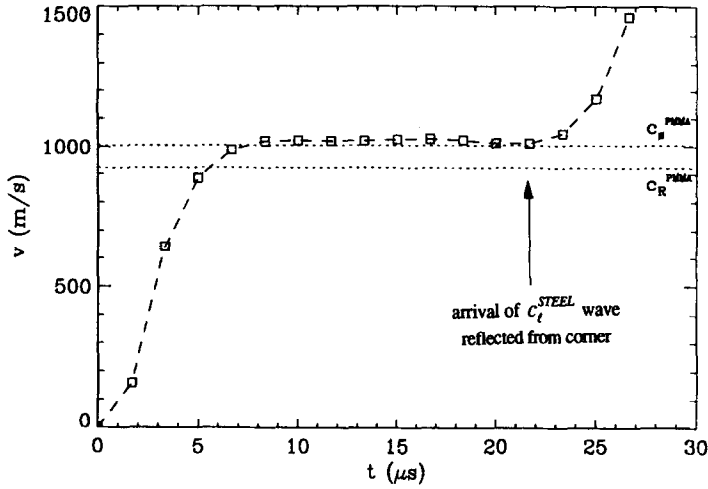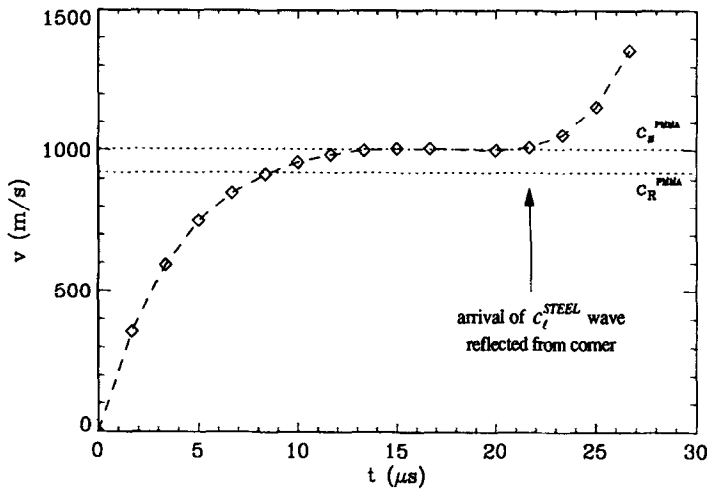contact region *d*

Fig. 7. Enlarged view of last frame of Fig. 5. Region over which crack face contact is believed to occur is denoted by *d*.

Fig. 6(a),(b). Typical velocity histories of one point bend air gun tests on two PMMA/steel specimens (sharp starter crack used).

possible for the interface to sustain crack propagation at a speed in the range $c_s^{PMMA} < v < c_l^{PMMA} < c_R^{STEEL}$ by having the steel side supply energy to the PMMA and still provide the crack tip with enough energy to create new surfaces. Overall the composite specimen will be losing energy, which brings it to a more favorable state. An alternative presentation of this behavior is possible. As the bond fractures, the PMMA side feels the effect as a traveling traction distribution on its surface. If the interface debonds fast enough, the traction distribution felt by the Plexiglas will be traveling on its surface at intersonic, or even supersonic, speeds (for Plexiglas). For the steel side however the debonding that is occurring is doing so at speeds still below
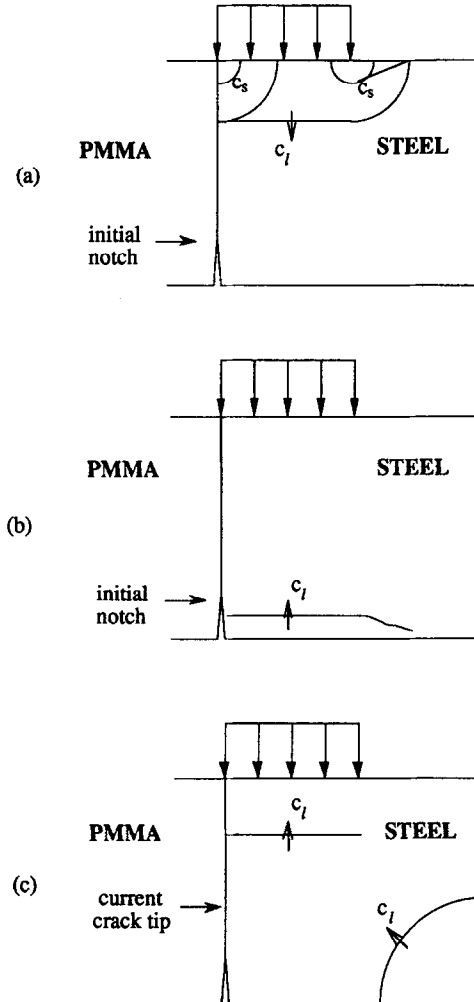
Fig. 8. Schematic describing the predominant interactions of stress waves with the interfacial crack tip, (a) just after impact, (b) just before crack initiation and (c) after crack growth.

its own Rayleigh wave speed. It seems energetically logical that an interfacial crack could under no circumstances exceed the Rayleigh wave speed of steel. It is believed that the maximum crack tip speed possible would be somewhere between c_l^{PMMA} and c_R^{STEEL}. It would be the velocity at which the steel side would no longer be able to supply energy to the PMMA and keep the crack moving.

It is possible to see the effect that waves traveling in the steel side of the specimen have on crack initiation in Fig. 8. A few microseconds after impact the waves propagating in the steel side of the specimen will be as shown in Fig. 8(a). At this stage the main compressive dilatational wave induces a downwards displacement in the steel side of the specimen that is parallel to the interface, while the PMMA side is essentially unaffected. The additional unloading waves seen in Fig. 8(a) are necessary to keep the portion of the steel surface that has not been impacted traction free. When

the main compressive plane wave reaches the pre-existing crack tip it will generate a state of shear around it because of the downwards displacement it induces in the steel side. Subsequently it will reflect off the bottom surface of the specimen as tension and reload the crack tip as seen in Fig. 8(b). The deformation induced now is again shearing and in the same sense as before. At this stage therefore the crack tip region is under severe shearing conditions. Essentially the steel side has slipped significantly with respect to the PMMA side which has not really been affected. If the intensity of the initial compressive wave is high enough (which is directly proportional to impact speed) the crack can initiate propagation even though in a state of shear. This is indeed what happens in the gas gun tests were the impact speed is 20 m s^{-1}. In fact the experimentally measured initiation time of 30 μs after impact correlates very well with the time it takes a dilatational wave in steel to travel the height of the specimen, reflect off the bottom surface and reach the initial crack tip.

In similar experiments where a lower impact speed was used (see Lambros and Rosakis, 1994b) crack tip initiation was not seen to occur until the unloading waves from the lower right hand corner of the steel side reached the crack tip, some 70–80 μs after impact [see Fig. 8(c)]. The reason for this delay was due to the lower impact speeds used in those experiments. In these low impact speed experiments, not described here, the stress field at 30 μs after impact was still shear dominated, but did not have a high enough magnitude to initiate the crack. Instead the crack had to wait until it was enveloped by a more opening mode type of stress field before it initiated. Mathematically the conditions for crack tip initiation in the two different kinds of tests, can be expressed as two different combinations of phase angle (or mixity) ϕ and energy release rate G. The phase angle is defined as $\phi = \tan^{-1}((\sigma_{22}/\sigma_{12})_{\substack{\theta=0 \\ r=\hat{r}}})$ and G is the energy released per unit crack advance. For a phase angle corresponding to a more shear dominated stress field, a larger G (and therefore impact speed) is necessary to cause initiation. In the case when initiation is delayed, as in the low impact speed experiments in Lambros and Rosakis (1994b), the crack tip initiates at a smaller value of the energy release rate, but under more opening mode conditions than the present experiments. This means that there is less energy available to drive the dynamically propagating crack and therefore propagation speeds are smaller. Indeed as can be seen in the work of Lambros and Rosakis (1994b), in one point bend tests having an impact speed of 4 m s^{-1} the crack tip speed approached but never exceeded c_R^{PMMA}.

A quantitative analysis of the fringe patterns in the subsonic regime of crack growth is possible as detailed in Lambros and Rosakis (1994a,b). A fit of the theoretically predicted asymptotic near tip stress field can be performed to the experimentally obtained interferograms. From such a fit we can obtain the time variation of the complex stress intensity factor, K^d, for each experiment. Using the time histories of K^d it is possible to deduce the time variation of crack face displacements behind the propagating crack tip. From the asymptotic expression of the displacement behind the propagating crack tip, the shearing δ_1 and opening δ_2 displacements can be written as (see Lambros and Rosakis, 1994b),

$$\delta_1(r) = \frac{H_{22}}{\cosh(\pi\varepsilon)} \sqrt{\frac{2r}{\pi}} \frac{|K^d|}{\sqrt{1+4\varepsilon^2}} \frac{1}{\eta} \sin(\phi + \varepsilon \ln r - \tan^{-1}(2\varepsilon)),$$

and

$$\delta_2(r) = \frac{H_{22}}{\cosh(\pi\varepsilon)} \sqrt{\frac{2r}{\pi}} \frac{|K^d|}{\sqrt{1+4\varepsilon^2}} \cos(\phi + \varepsilon \ln r - \tan^{-1}(2\varepsilon)). \tag{5}$$

Quantities ε and η are interface parameters that depend on material properties and crack tip speed. (ε is the well known oscillatory index.) The function H_{22} is given in Yang *et al.* (1991) and is also a function of material properties and crack tip speed. $|K^d|$ is the magnitude of the complex stress intensity factor, ϕ is the phase angle and v is the crack tip speed. The ratio of displacements can then be computed as

$$\frac{\delta_1}{\delta_2}(r) = \frac{1}{\eta} \tan(\phi + \varepsilon \ln r - \tan^{-1}(2\varepsilon)). \tag{6}$$

Therefore, having experimentally measured values of ϕ allows us to compute δ_1/δ_2 at some distance $r = a$ behind the crack tip. This has been done in Lambros and Rosakis (1994b). Figure 9(a) shows a plot of experimentally obtained data points of velocity and phase angle for subsonic crack growth. These are for tests performed at an impact speed of 4 m s^{-1}. The line superposed in Fig. 9(a) is obtained by setting the displacement ratio given in (6) to a constant value C_1 and choosing C_1 to fit the experimental data. Figure 9(b) shows a similar plot for the subsonic portion of the gas gun tests described earlier, which used an impact speed of 20 m s^{-1}. The fact that δ_1/δ_2 seems to remain constant throughout propagation in both cases was used in Lambros and Rosakis (1994b) to propose a fracture criterion for dynamic crack growth along bimaterial interfaces. In the current study we are interested in the value of the constant C_1 in each of the two cases. In Fig. 9(a) C_1 has a value of -0.3. This signifies that the shearing displacement δ_1 is 30% of the opening displacement δ_2. Therefore, in the case corresponding to the results shown in Fig. 9(a), crack growth occurs in a primarily opening mode. On the other hand, C_1 from Fig. 9(b) can be seen to have a value of -3. In this case the ratios of δ_1 and δ_2 are reversed and crack growth occurs in a primarily shear mode. The gas gun experiments with 20 m s^{-1} impact speed lead therefore to a predominately shear dominated crack growth process. It is this shear dominated process that is directly responsible for the attainment of transonic crack growth speeds in these experiments. The amounts of energy necessary to initiate the crack at these shear dominated mixities are so large that the crack tip is eventually driven to run at intersonic speeds.

The theoretical near tip fields used for the above analysis have been well established for the sub-Rayleigh regime of bimaterial crack growth (Yang *et al.*, 1991; Deng, 1992; Liu *et al.* (1993)). In addition, for cracks propagating in the regime $c_R^{PMMA} < v < c_s^{PMMA}$ the leading order of the stress field surrounding the crack tip was obtained by Liu *et al.* (1993). For convenience the results of this derivation are repeated in Part II of this work. One of their results was that the energy release rate is zero in this regime of crack propagation velocity. Figure 10 shows the variation of energy release rate with velocity for the sub-Rayleigh regime of the one point bend impact tests. Even though we do not have a good enough resolution to distinguish between crack propagation at c_R^{PMMA} or c_s^{PMMA} (i.e. 920 and 1000 m s^{-1}) it is clear from this plot that the energy release rate does indeed seem to fall to zero as the Rayleigh wave speed of PMMA is approached by the propagating crack tip.
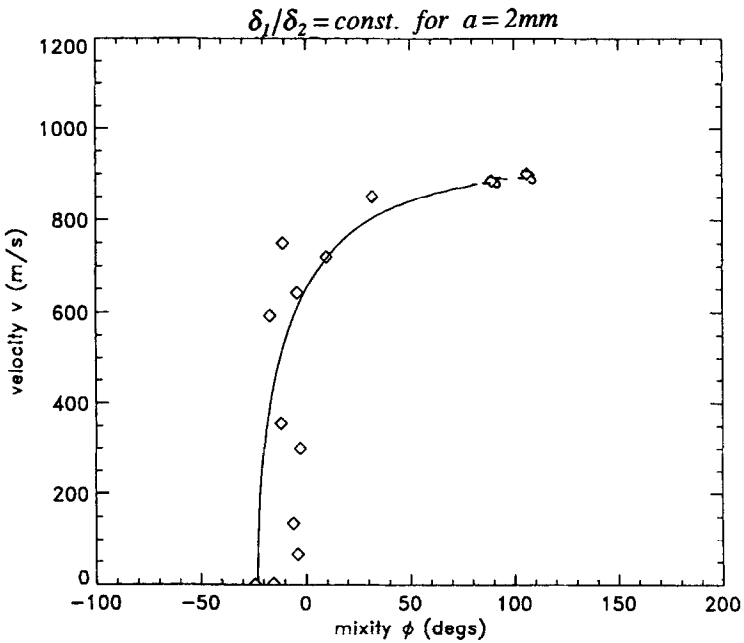
(a)

$\delta_1/\delta_2 = const.$ for $a = 2mm$

(b)

$\delta_1/\delta_2 = const.$ for $a = 2mm$
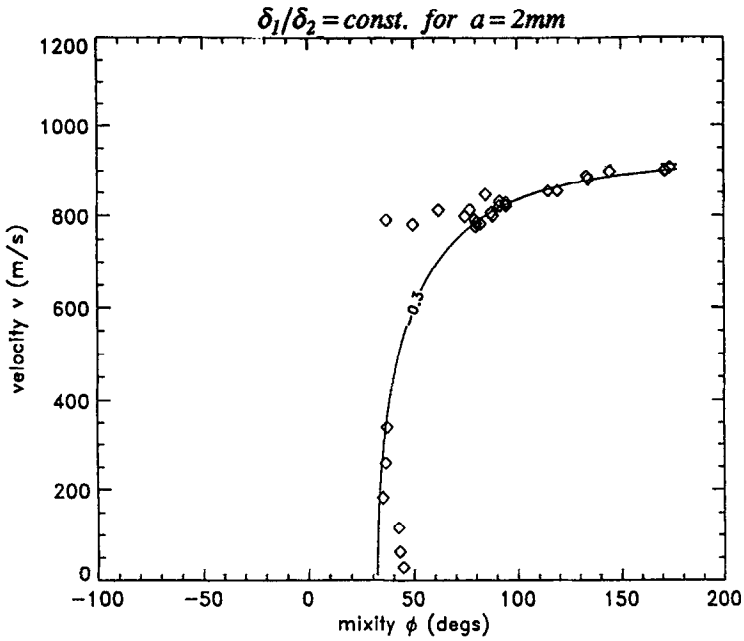
Fig. 9. (a) Variation of mixity ϕ with crack tip velocity v. Data points correspond to low velocity impact, drop weight tower experiments. Solid line corresponds to constant $\delta_1/\delta_2 = -0.3$. (b) Variation of mixity ϕ with crack tip velocity v. Data points correspond to high velocity impact, gas gun experiments. Only the sub-Rayleigh portion of crack growth is shown. Solid line corresponds to constant $\delta_1/\delta_2 = -3$.
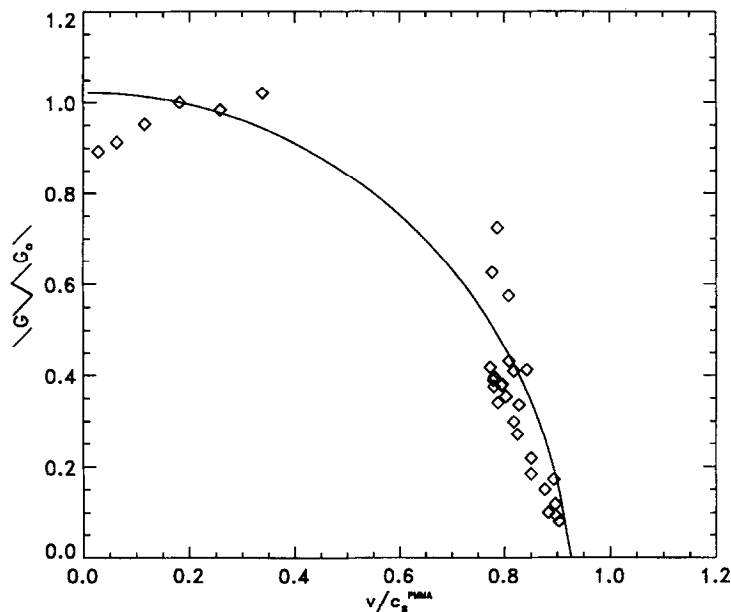
Fig. 10. Normalized energy release rate from the PMMA/steel one point bend experiments vs crack tip speed v (sub-Rayleigh crack growth regime).

3.2. Comparison of experiments with the intersonic analysis of Part II

Up until recently, there was no theoretical analysis available for a bimaterial crack propagating at speeds in excess of c_s^{PMMA}. This issue is addressed by the second part of this work. There it has been concluded that it is impossible to concurrently have opening stresses ahead of the crack tip and opening displacements behind it, when the crack tip speed is in the regime between c_s^{PMMA} and $\sqrt{2}\,c_s^{PMMA}$. This would imply that dynamic crack growth in this regime would result in crack face closure, which could be unfavorable for continued stable crack propagation. Indeed, intuitively stable crack growth conditions would require that both normal stresses ahead of the tip and crack face displacements behind it be positive at the same time. On the other hand, above a crack tip speed of $\sqrt{2}\,c_s^{PMMA}$ the theoretical solution predicts crack propagation occurring with both opening stresses ahead and opening displacements behind the crack tip. Intuitively this may imply a more favorable crack propagation regime.

The velocity profiles obtained in the current experiments seem to be consistent with these results. Looking at Fig. 6(a) and (b) we see that the measured crack tip speed reaches a plateau at about $1000\ \mathrm{m\ s^{-1}}(\approx c_s^{PMMA})$. It does not seem to be able to have enough energy to cross this barrier until several microseconds later. For that period it remains propagating at c_s^{PMMA} which is the last favorable propagation velocity before the, theoretically predicted, unfavorable regime. When the velocity increases again it very quickly (accelerations of $10^8\ \mathrm{m\ s^{-2}}$) grows to values over $1400\ \mathrm{m\ s^{-1}}$ ($\approx \sqrt{2}c_s^{PMMA}$). It is interesting to note that the time at which this acceleration occurs coincides with the arrival time of a dilatational stress wave reflected from the specimen corner [see Figs 8(c) and 6(a) and (b)]. This dilatational wave, which approaches the

propagating crack at about 75°, introduces a larger opening component to the crack face displacements than before, and provides the energy necessary for the crack tip speed to cross over from c_s^{PMMA} to the next favorable crack growth regime. The experimental evidence therefore seems to reinforce the conclusion that there indeed exists an unfavorable region for stable crack growth in this bimaterial system between speeds of c_s^{PMMA} and $\sqrt{2}c_s^{PMMA}$. This region is one in which crack propagation is possible, but unstable, and the interfacial crack wants to quickly accelerate out of it. There are several frames in our optical experiments that correspond to crack propagation in the unfavorable velocity regime (i.e. c_s^{PMMA} to $\sqrt{2}c_s^{PMMA}$). An example is the last frame seen in Fig. 5 and enlarged in Fig. 7. As was mentioned earlier the peculiarities of this fringe pattern, and in particular the behavior along length d, are believed to be because of crack face contact behind the propagating tip. This is actually in agreement with the theoretical predictions of Part II where it is seen that, when the crack is traveling at speeds between c_s^{PMMA} and $\sqrt{2}c_s^{PMMA}$, crack closure is predicted if there are to be opening stresses ahead of the crack. The size of the contact region in Fig. 7 is $d = 1.67$ mm.

The above phenomenon, i.e. of having favorable and unfavorable stable crack propagation velocity ranges, is very similar to results for homogeneous materials that were seen in the work of Andrews (1976). In that work, Andrews performed numerical calculations on plane strain cracks propagating under predominately shear conditions. By assuming a particular type of shear process zone ahead of the crack tip and by imposing a combination of critical energy release rate and critical opening stress as a fracture criterion, he calculated the crack tip propagation velocity history. He found that stable crack growth could occur only in the regimes $0 < v < c_R$ and $\sqrt{2}c_s < v < c_l$.

The fact that such behavior seems to occur under primarily shear dominated crack growth, in both the homogeneous and bimaterial cases, makes the above results important when considering ruptures along earthquake faults. Indeed as mentioned by Freund (1990) in section 4.3 of his book on dynamic fracture: "Analysis of seismic data taken during crustal earthquakes has led to the conclusion that a shear fracture on a pre-existing fault can propagate at a speed greater than the shear wave speed of the crustal material Archuleta (1982)". As shown in Fig. 8(a) and (b) crack initiation in our experimental configuration occurs under predominately shear conditions, a situation which seems to mimic the initiation of rupture along an earthquake fault. In addition, the observation of limited contact, even in the absence of overall confining pressures, is reminiscent of current models of fault rupture as described by Heaton (1990).

ACKNOWLEDGEMENTS

REFERENCES

Aleksandrov, V. M. and Smetanin, B. I. (1990) Supersonic cleavage of an elastic strip. *Appl. Math. Mech.* **54**(5), 677–682.

Andrews, D. J. (1976) Rupture velocity of plane strain shear cracks. *J. Geophys. Res.* **81**(32), 5679–5687.

Archuleta, R. J. (1982) Analysis of near-source static and dynamic measurements from the 1979 Imperial Valley earthquake. *Bull. Seismological Soc. Am.* **72**(6), 1927–1956.

Atkinson, C. (1977) Dynamic crack problems in dissimilar media. *Mechanics of Fracture-4*: *Elastodynamic Crack Problems* (ed. G. Sih.), Vol. 4, pp. 213–248. Martinus Nijhoff, The Netherlands.

Broberg, K. B. (1960) The propagation of a Griffith crack. *Ark. Fys.* **18**, 159.

Broberg, K. B. (1985) Irregularities at earth-quake slip. *J. Tech. Phys.* **26**(3–4), 275–284.

Broberg, K. B. (1989) The near-tip field at high crack velocities. *Int. J. Fract.* **39**(1–3), 1–13.

Broberg, K. B. (1993) Intersonic Mode II Crack Expansion, private communication.

Brock, L. M. and Achenbach, J. D. (1973) Extension of an interface flaw under the influence of transient waves. *Int. J. Solids Struct.* **9**, 53–67.

Burridge, R., Conn, G. and Freund, L. B. (1979) The stability of a rapid mode II shear crack with finite cohesive traction. *J. Geophys. Res.* **85**(B5), 2210–2222.

Bykovtsev, A. S. and Kramarovskii, D. B. (1989) Non-stationary supersonic motion of a complex discontinuity. *Appl. Math. Mech.* **53**(6), 779–786.

Curran, D. R., Shockey, D. A. and Winkler, S. (1970) Crack propagation at supersonic velocities, II. Theoretical model. *Int. J. Fract.* **6**(3), 271.

Deng, X. (1992) Complete complex series expansions of near tip fields for steadily growing interface cracks in dissimilar isotropic materials. *Engng Fract. Mech.* **42**(2), 237–242.

Freund, L. B. (1990) *Dynamic Fracture Mechanics*. Cambridge University Press, Cambridge.

Goldshtein, R. V. (1967) On surface waves in joined elastic materials and their relation to crack propagation along the junction. *Appl. Math. Mech.* **31**, 496–502.

Heaton, T. H. (1990) Evidence for and implications of self-healing pulses of slip in earthquake rupture. *Phys. Earth Planetary Interiors* **64**, 1–20.

Lambros, J. and Rosakis, A. J. (1994a) Dynamic decohesion of bimaterials: experimental observations and failure criteria. To appear in a special volume of the *Int. J. Solids Struct.* devoted to Dynamic Failure of Modern Materials.

Lambros, J. and Rosakis, A. J. (1994b) On the development of a dynamic decohesion criterion for bimaterials. Submitted to the *Proc. R. Soc. Lond.*

Lee, Y. J., Lambros, J. and Rosakis, A. J. (1994) Analysis of Coherent Gradient Sensing (CGS) by Fourier optics. Submitted to *Optics Lasers Engng.*

Lee, Y. J. and Rosakis, A. J. (1993) Interfacial cracks in plates: a three dimensional numerical investigation. *Int. J. Solids Struct.* **30**(22), 3139–3158.

Liu, C., Lambros, J. and Rosakis, A. J. (1993) Highly transient elastodynamic crack growth in a bimaterial interface: higher order asymptotic analysis and experiments. *J. Mech. Phys. Solids* **41**(12), 1887–1954.

Rosakis, A. J. (1993) Two optical techniques sensitive to gradients of optical path difference: The method of caustics and the coherent gradient sensor (CGS). *Experimental Techniques Fracture*, pp. 327–425.

Tippur, H. V. (1992) Coherent gradient sensing: A Fourier optics analysis and applications to fracture. *Appl. Optics* **31**(22), 4428–4439.

Tippur, H. V., Krishnaswamy, S. and Rosakis, A. J. (1991) A coherent gradient sensor for crack tip measurements: analysis and experimental results. *Int. J. Fract.* **48**, 193–204.

Tippur, H. V. and Rosakis, A. J. (1991) Quasi-static and dynamic crack growth along bimaterial interfaces: a note on crack-tip field measurements using coherent gradient sensing. *Exp. Mech.* **31**(3), 243–251.

Willis, J. R. (1971) Fracture mechanics of interfacial cracks. *J. Mech. Phys. Solids* **19**, 353–368.

Willis, J. R. (1973) Self-similar problems in elastodynamics. *Phil. Trans. R. Soc. (Lond.)* **274**, 435–491.

Winkler, S., Shockey, D. A. and Curran, D. R. (1970) Crack propagation at supersonic velocities, I. *Int. J. Fract.* **6**(2), 151.

Yang, W., Suo, Z. and Shih, C. F. (1991) Mechanics of dynamic debonding. *Proc. R. Soc. Lond.* **A433**, 679–697.